8-1-2017

Time-Restricted Feeding Shifts the Skin Circadian Clock and Alters UVB-Induced DNA Damage.

Hong Wang

Elyse van Spyk

Qiang Liu

Mikhail Geyfman

Michael L Salmans

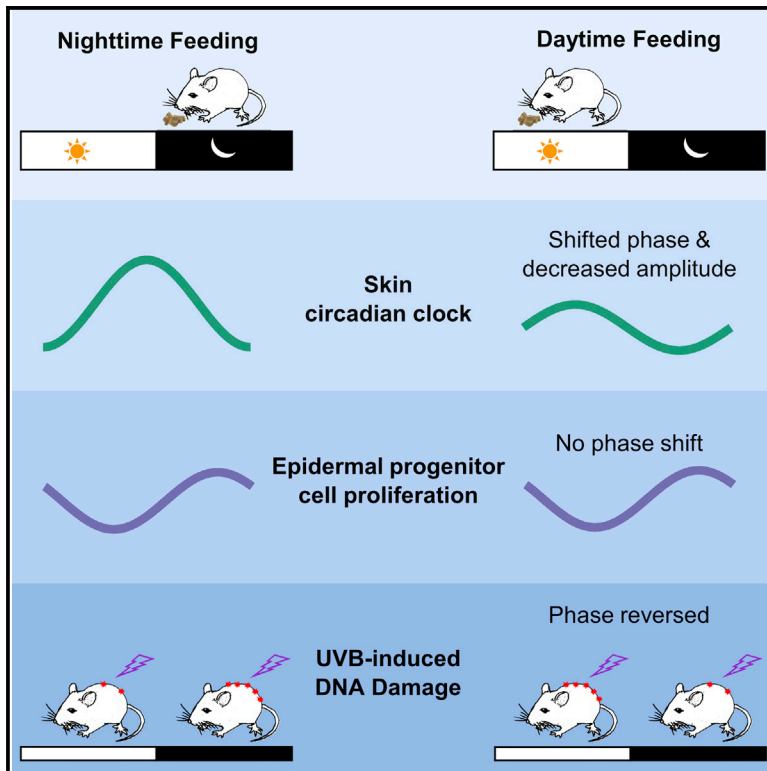*See next page for additional authors*

Recommended Citation

Authors

Hong Wang, Elyse van Spyk, Qiang Liu, Mikhail Geyfman, Michael L Salmans, Vivek Kumar, Alexander Ihler, Ning Li, Joseph S Takahashi, and Bogi Andersen

Time-Restricted Feeding Shifts the Skin Circadian Clock and Alters UVB-Induced DNA Damage

Graphical Abstract

Highlights

- Restricted feeding (RF) alters the phase and amplitude of the skin circadian clock

- Food intake acutely alters the expression of many genes in the skin

- RF affects the rate but not the phase of epidermal progenitor diurnal proliferation

- Daytime RF reverses diurnal sensitivity to UVB-induced DNA damage

Authors

Hong Wang, Elyse van Spyk, Qiang Liu, ..., Ning Li, Joseph S. Takahashi, Bogi Andersen

Correspondence

bogi@uci.edu

In Brief

Little is known about the effect of time of feeding on skin function. Wang et al. find that time-restricted feeding schedules affect skin gene expression, epidermal progenitor cell proliferation, and UVB-induced DNA damage, pointing to a modulatory role for food-intake timing in skin biology.

Accession Numbers

GSE83855

CrossMark

CellPress

Time-Restricted Feeding Shifts the Skin Circadian Clock and Alters UVB-Induced DNA Damage

Hong Wang,[1,2,3,13] Elyse van Spyk,[2,13] Qiang Liu,[4,11] Mikhail Geyfman,[2,12] Michael L. Salmans,[2] Vivek Kumar,[5] Alexander Ihler,[4] Ning Li,[1] Joseph S. Takahashi,[6,7] and Bogi Andersen[2,8,9,10,14,*]
[1]State Key Laboratory for Agrobiotechnology, College of Biological Sciences, China Agricultural University, Beijing 100193, China
[2]Department of Biological Chemistry, University of California, Irvine, Irvine, CA 92697, USA
[3]Department of Cell Biology and Genetics, School of Preclinical Medicine, Guangxi Medical University, Nanning 530021, China
[4]Department of Computer Science, University of California, Irvine, Irvine, CA 92697, USA
[5]The Jackson Laboratory, Bar Harbor, ME 04609, USA
[6]Department of Neuroscience
[7]Howard Hughes Medical Institute
University of Texas Southwestern Medical Center, Dallas, TX 75390, USA
[8]Department of Medicine, Division of Endocrinology, School of Medicine
[9]Center for Complex Biological Systems
[10]Institute for Genomics and Bioinformatics
University of California, Irvine, Irvine, CA 92697, USA
[11]Present address: Department of Computer Science, Dartmouth College, Hanover, NH 03755, USA
[12]Present address: Department of Biology, Allergan, Inc., Irvine, CA 92612, USA
[13]These authors contributed equally
[14]Lead Contact
*Correspondence: bogi@uci.edu
http://dx.doi.org/10.1016/j.celrep.2017.07.022

SUMMARY

The epidermis is a highly regenerative barrier protecting organisms from environmental insults, including UV radiation, the main cause of skin cancer and skin aging. Here, we show that time-restricted feeding (RF) shifts the phase and alters the amplitude of the skin circadian clock and affects the expression of approximately 10% of the skin transcriptome. Furthermore, a large number of skin-expressed genes are acutely regulated by food intake. Although the circadian clock is required for daily rhythms in DNA synthesis in epidermal progenitor cells, RF-induced shifts in clock phase do not alter the phase of DNA synthesis. However, RF alters both diurnal sensitivity to UVB-induced DNA damage and expression of the key DNA repair gene, *Xpa*. Together, our findings indicate regulation of skin function by time of feeding and emphasize a link between circadian rhythm, food intake, and skin health.

INTRODUCTION

Acting as a strong barrier to physical, chemical, and pathogenic insults from the exterior, and to water loss from the interior, the epidermis, the outermost layer of the skin, is a stratified epithelium. Its homeostasis is balanced by stem cell progeny production in the basal layer and loss of cells through terminal differentiation culminating in shedding of corneocytes at the skin's

surface (Blanpain and Fuchs, 2009). Skin biology research focuses largely on the responses to various forms of external injury, including UV irradiation, a major cause of DNA damage, accelerated skin aging, and cancer (Armstrong and Kricker, 2001; Fisher et al., 2002). Recent work, however, has unearthed an important role for the circadian clock in regulating skin function (Plikus et al., 2015). This raises the intriguing possibility that signals that influence circadian clocks, such as the time of feeding, could act as a regulator of skin function; the clocks in some peripheral tissues, especially metabolic organs, including the liver, can be entrained by time-restricted feeding (RF) (Damiola et al., 2000; Hara et al., 2001; Izumo et al., 2014; Kuroda et al., 2012; Stokkan et al., 2001).

The hierarchically organized mammalian circadian clock comprises the central clock, located in the suprachiasmatic nucleus (SCN), and peripheral clocks, possessed by almost all cells (Dibner et al., 2010; Mohawk et al., 2012). Entrained by the day-night cycle, the central clock synchronizes the phases of peripheral clocks, thus coordinating the locomotor and metabolic activity of the animal with the Earth's rotation. At a molecular level, the central and peripheral clocks are transcription-translation feedback loops wherein the heterodimeric CLOCK/BMAL1 transcription complex activates a large number of genes. These include PERs and CRYs that form heterodimers to inhibit CLOCK/BMAL1 activity, thus establishing an oscillating transcriptional output with 24 hr periodicity (Dibner et al., 2010; Lowrey and Takahashi, 2011; Mohawk et al., 2012). The direct and indirect targets of the circadian clock encode key regulators of many, if not most, biological processes, including metabolism (Bass, 2012; Lamia et al., 2011), cell proliferation (Lévi et al., 2007; Masri et al., 2013),

and response to therapeutic treatment (Lévi et al., 2007; Levi and Schibler, 2007).

Previous studies showed important roles for the circadian clock in skin biology (Plikus et al., 2015). The clock is highly active in the progenitor cells of the secondary hair germ, where it plays a role in the initiation of the hair growth cycle (Lin et al., 2009). It also contributes to heterogeneity in hair follicle stem cells by regulating the sensitivity to activation signals (Janich et al., 2011). In addition, in the matrix of growing hair follicles, the clock determines diurnal variation in cell division, which affects the sensitivity of hair follicles to external gamma radiation (Plikus et al., 2013). The circadian clock also gates the response to UVB radiation in the skin (Gaddameedhi et al., 2011; Geyfman et al., 2012), at least in part by controlling the expression of *Xpa*, a rate limiting enzyme involved in the repair of UVB-induced DNA damage (Gaddameedhi et al., 2011; Kang et al., 2010). In fact, the skin is most sensitive to UVB-induced tumor induction at night, when expression of *Xpa* is lowest (Gaddameedhi et al., 2011). Studies also showed a link between the circadian clock and skin aging as *Bmal1*-deleted mice exhibit accelerated skin aging (Janich et al., 2011; Kondratov et al., 2006), perhaps related to excessive reactive oxygen species (ROS) generation. In the interfollicular epidermal progenitor cells, the clock is required for a prominent diurnal variation in DNA synthesis (Gaddameedhi et al., 2011; Geyfman et al., 2012). Although the function of these diurnal rhythms in epidermal progenitor cell DNA synthesis remains unknown, transcriptome studies from yeast to mammals have suggested that the circadian clock may coordinate the timing of different cellular processes (Geyfman et al., 2012; Gillette and Sejnowski, 2005; Jouffe et al., 2013; Panda et al., 2002); in the case of epidermal progenitor cells, its role may be to synchronize intermediary metabolism and the cell cycle, thus minimizing cellular damage from oxidative phosphorylation-generated ROS (Stringari et al., 2015). The circadian clock, then, may be a mediator of the long-appreciated yet incompletely understood crosstalk between metabolism and the cell cycle (Buchakjian and Kornbluth, 2010; Fritz and Fajas, 2010; Laporte et al., 2011).

Despite the circadian clock's multiple roles in skin biology, other than the SCN, little is known of the factors that entrain the skin circadian clock. Restriction of food intake to defined time periods is known to change the phase of the circadian clock and gene expression programs, especially in primary metabolic organs such as the liver (Adamovich et al., 2014; Damiola et al., 2000; Kuroda et al., 2012; Stokkan et al., 2001). But not all peripheral tissues are entrained by RF (Izumo et al., 2014), and the effect of RF on the skin has not been investigated. Hence, we examined whether RF can entrain the circadian clock in skin and affect skin function. We discovered that RF can shift the circadian clock of skin but that the phase of the skin circadian clock is not as tightly coupled to feeding time (FT) as that of the liver. We found RF schedule-specific changes in the skin transcriptome, including changes in the expression of multiple metabolic genes and the nucleotide excision repair factor, *Xpa*. Although the phase of the cell cycle was insensitive to changes in circadian clock phase, RF decreased overall progenitor proliferation rates, and daytime RF reversed diurnal rhythm of epidermal sensitivity to UVB-induced DNA damage. This study points to unexpected influences of time of feeding on the biology of skin, suggesting that time of feeding may affect UVB-induced conditions such as skin cancer and premature aging.

RESULTS

RF Entrains the Skin Circadian Clock in a Manner Distinct from that of the Liver

To determine whether RF can shift the phase of the skin circadian clock, we administered five different feeding schedules (Figure 1A). The ad libitum (AD) group of mice had unlimited access to food. The early daytime (ED) feeding group had access to food from zeitgeber time (ZT) 0 for 4 hr. The midday (MD) feeding group had access to food from ZT5 for 4 hr. The early nighttime (EN) feeding group had access to food starting at ZT12. Finally, the long daytime (LD) feeding group had access to food from ZT3 for 8 hr. These feeding lengths and times were modeled on previous RF studies (Damiola et al., 2000; Stokkan et al., 2001).

To evaluate the effect of RF schedules on body weight and food intake, we recorded food intake daily and body weight immediately prior to food availability every other day for 21–26 days for the AD, EN, MD, and ED groups (Figures S1A and S1B). Both MD and ED mice ate significantly less than the AD mice during the first 2 days of RF, but by the end of the experiment, there was no significant difference in food intake across the groups (Figure S1A). All groups weighed approximately the same prior to the beginning of the RF (data not shown), but throughout the RF experiment, body weight was significantly affected by RF schedule: AD weighed more than all RF groups, ED and EN had approximately equal body weight, and MD weighed consistently less than all other groups (Figure S1B). We performed two RF experiments as described in Experimental Procedures, with similar results for body weight and food intake in both experiments (data not shown). We also measured skin compartment width (epidermis; dermis, including dermal fat layer; and muscle layer) by histology and found no significant changes except that dermis width was decreased by about 16%–17% in EN and MD compared with AD (Figures S1C–S1F).

After implementing these RF schedules for 18–21 days, we harvested skin and liver from cohorts of mice every 4 hr for 28 hr starting at ZT0. We then determined the circadian clock phase by analyzing the peak time of skin mRNA expression of *Per2*, a commonly used indicator of circadian phase. The phase of *Per2* in mice fed during the night (EN) was equivalent to that of AD (Figure 1B). Using AD as a reference, we found that MD induced a phase advance on average of 4.19 ± 0.43 hr; in contrast, ED caused a phase delay on average of 4.72 ± 0.38 hr (Figures 1C and S2A). The phase of *Per2*, then, was almost 9 hr apart for MD and ED, the groups with the most widely separated phases (Figure 1B). The magnitude of phase advances was the same in LD and MD (Figure S2A). We also found that the amplitude of *Per2* was significantly lower in day-fed mice compared with EN (Figure 1C). Using either AD or EN as a reference, the phase shift of *Per2* in ED was significantly different compared with LD and MD (Figure S2A). By contrast, in the liver, the phase of *Per2* expression in all feeding groups was tightly linked to the time of initiation of food intake
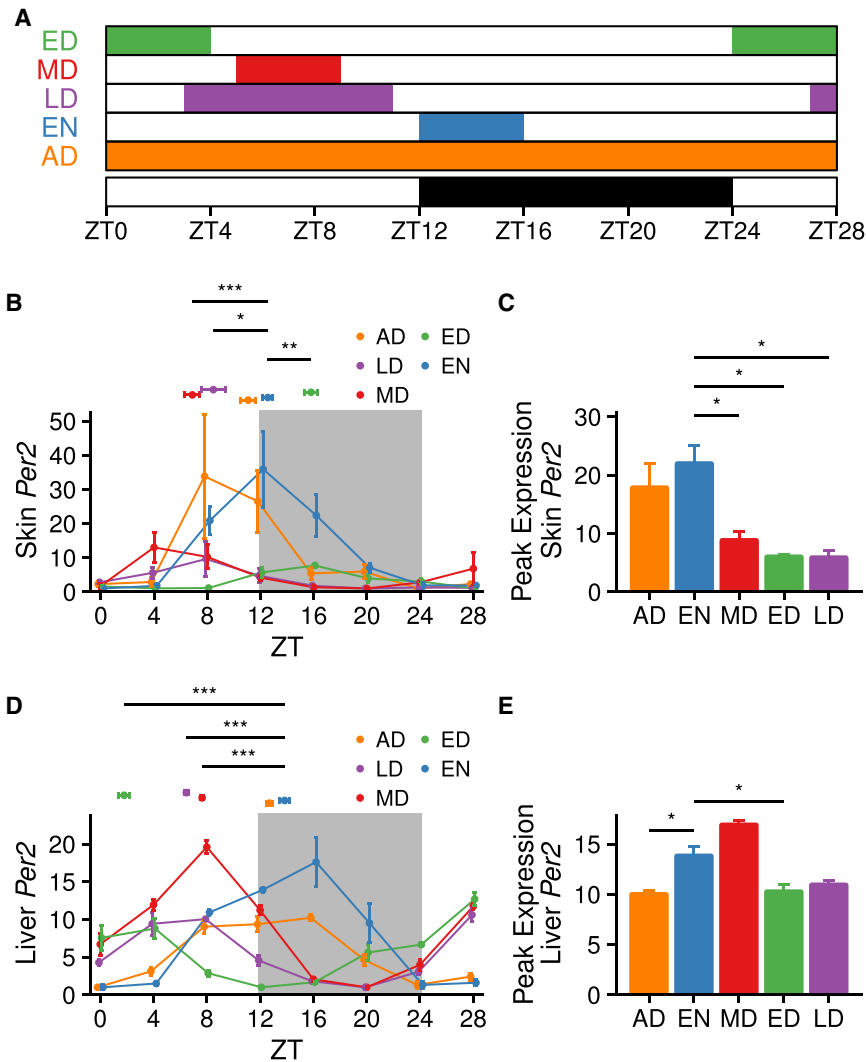
Diverse but Functionally Similar Diurnal Transcriptomes under Different RF Schedules

To define the diurnal transcriptome of skin under different RF schedules, we performed RNA sequencing (RNA-seq) on telogen skin collected every 4 hr for 28 hr under the three 4 hr RF schedules: ED, MD, and EN (Figure 1A; Table S1). We selected mice from these RF schedules for further study in order to minimize effects of differences in caloric intake (see Experimental Procedures). EN mice were selected as the control because their circadian phase and time of feeding is similar to that of AD mice (Figures 1A and 1B); AD mice feed mainly during the early night (Vollmers et al., 2009; Yoon et al., 2012). Analysis of ED and MD mice allows us to observe the effect of maximum diurnal phase shifts as their circadian phases are nearly 9 hr apart in skin (Figures 1B and S2A).

To quantify RNA expression levels, we separately counted the reads in exons, introns, and antisense strands of all genes in the University of California, Santa Cruz (UCSC), canonical gene set (Figure S3A). Using a combination of four algorithms (Figure S3B), we identified 2,997, 3,198, and 2,546 exon transcripts as diurnally oscillating (among 22,583 detected) in the EN, ED, and MD groups, respectively (Figure 2A; Table S2). Surprisingly, for each feeding group, there was a large number of genes with diurnally oscillating expression unique to that group, and only 147 genes were common to all three feeding groups (Figure 2A; Table S2). These common genes include the core clock regulators *Clock*, *Cry1/2*, *Per2/3*, *Dbp*, and *Npas2* (Figure 2B; Table S2). The overall shift direction of the diurnal transcriptome common between any two RF schedules was consistent with the shift of the circadian clock (Figures 1B and 2B–2E; Table S2). Specifically, compared with EN, the phase of most diurnal

(Figures 1D and S2B), and the peak expression of neither ED nor LD was significantly different from EN (Figure 1E).

To determine if the shift in the phase of the circadian clock was consistent in the skin and liver, we compared the phase shift of *Per2* in the RF groups relative to AD or EN, and found that although MD exhibited the same phase advance in skin and liver, the phase shifts for ED and LD were different in these organs (Figure S2C). Expression results for core clock genes *Dbp* (Figures S2D–S2F) and *Per1* (Figures S2G–S2I) matched the *Per2* results, indicating a true phase shift of the core clock machinery. We also studied the phase and peak expression of *Per2* in isolated epidermis of EN and ED, finding that they are similar to that in whole skin (Figures S2J, S2K, 1B, and 1C).

Collectively, these data demonstrate that time of feeding influences the phase and peak expression of the skin circadian clock in manner distinct from that of the liver. Although feeding appears to be a direct zeitgeber for the liver with *Per2* expression having a constant relation to feeding time, there is a less direct relationship between the initiation of feeding and the phase of the skin circadian clock.

B

CD RO CC CL

Clock
Npas2
Arntl
Cry1
Per2
Nr1d1
Cry2
Per3
Nr1d2
Dbp

A

EN
2029

486 | **B** | 335

E | 147 | **C**

2258 | **D** | 1757

307

ED | MD

Color Key for B–E

−3 −2 −1 0 1 2 3

E

CD RO CC CL

486

400

300

200

100

1

C

CD RO CC CL

300

200

100

D
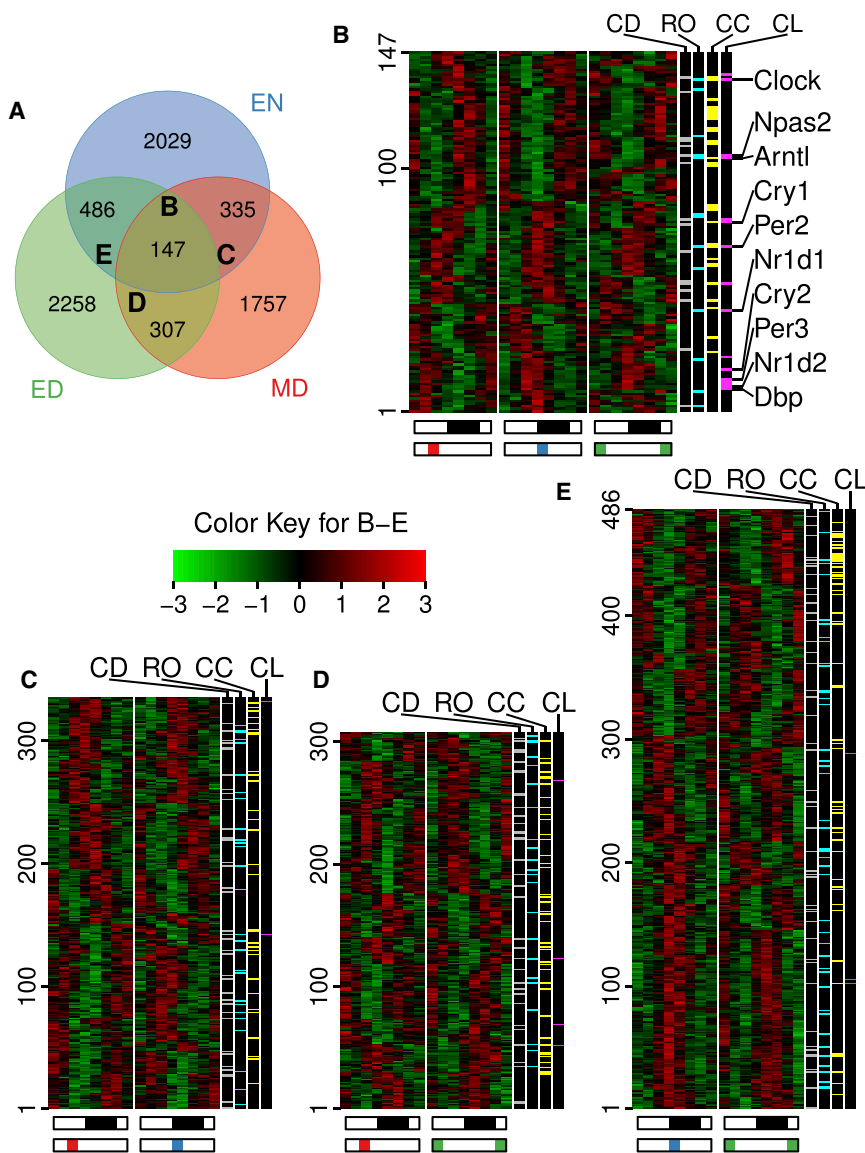
CD RO CC CL

300

200

100

1

Figure 2. Diurnal Transcriptome of Skin under Time-Restricted Feeding

(A) Venn diagram depicting the overlap of diurnal exons expressed in skin of mice after time-restricted feeding. Of 7,317 total diurnally oscillating exon transcripts, 147 are common within all 3 RF schedules. Exons for core circadian clock genes (such as *Clock*, *Npas2*, and *Arntl*) maintained diurnal rhythm in all RF schedules (core clock gene examples listed in [B], to the right).

(B–E) Heatmaps of the diurnal exons common under all (B) or two (C–E) of the RF schedules (corresponding to the B–E labels in [A]). Note that in (B), most genes in MD are phase advanced, while those in ED are phase delayed compared with EN. The white-black bars below indicate day and night, respectively. Colored bars under the heatmaps indicate the time of food availability. The color key for the heatmaps show the *Z* score of expression value, where red is highly expressed and green is minimally expressed. The colored lines in black bars to the right of the heatmaps indicate genes annotated to cell death (CD), reduction-oxidation (RO), cell cycle (CC), and circadian clock (CL) biological processes.

See also Table S1, Table S2, and Figure S3.

S3G; Table S2). This mode of regulation was reflected in our Gene Ontology (GO) analysis showing that the circadian clock genes are clearly regulated transcriptionally (Figure 3B). However, there were a number of genes that were exceptions to this general rule, as exemplified by cytokinesis genes, which appear to be regulated post-transcriptionally (Figure 3B).

We found only 37 antisense transcripts with diurnal expression in all three feeding schedules (Figure S3D). Some of these, including the clock regulator *Dec2* (also known as *Bhlhe41*), show expression in phase with the exons (Figure 3C) while others, including *Erc2*, which is involved

genes in MD advanced, while the phase of most diurnal genes in ED delayed (Figures 2C–2E; Table S2). Whereas the specific genes overlapping between any two groups differ, their functional categories were conserved, including cell death, redox regulation, cell cycle, and circadian clock (Figures 2B–2E; Table S2).

We also identified diurnal intron (Figure S3C; Table S2) and antisense (Figure S3D; Table S2) transcripts. Because transcription affects both intron and exon components of transcripts, the comparison of phase shifts between introns and exons in a gene gives insights into the extent to which the phases of diurnal genes and biological processes under different RF schedules are controlled at a transcriptional or a post-transcriptional level. Overall, we found that the phase shift in peak expression in exons and introns of a gene was correlated (Pearson R = 0.68), suggesting that transcriptional regulation is an important mechanism underlying food entrainment in the skin (Figures 3A and S3E–

in regulation of neurotransmitter release, show antiphasic expression to the exons (Figure 3D).

Together, these data indicate that RF shifts the phase of most diurnal genes in skin by transcriptional mechanisms. The RF-affected genes, although participating in similar functions, are largely unique to each RF schedule. In addition, we identified two antisense transcripts that may have a regulatory relationship with the gene from which they are encoded.

Food Intake Acutely Regulates a Portion of the Skin Transcriptome

We next considered the possibility that food intake could acutely affect skin gene expression. To search for such effects in the data, we rearranged the RNA-seq reads across all three feeding schedules according to the feeding time (Figure 4A), generating feeding time series (FT0–FT4–FT8), where FT0 represents the
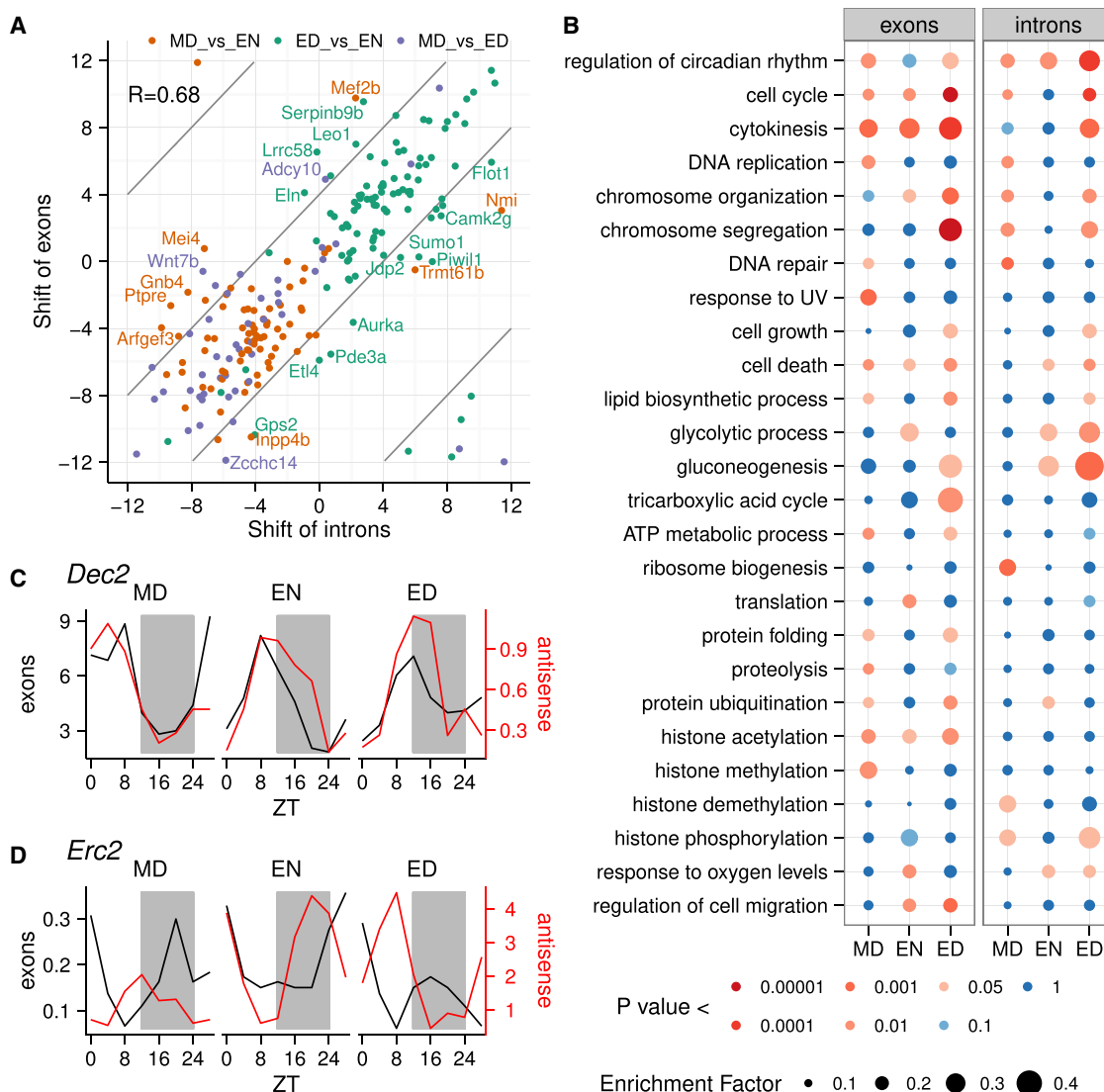
Figure 3. Functional and Regulatory Aspects of the Skin Diurnal Transcriptome

(A) Linear correlation of the time-shift of exon and intron expression under different RF schedules. Examples of genes for which the differential timing of intron and exon expression is greater than 4 hr are indicated with gene symbols.

(B) Enrichment of biological processes was determined for genes with diurnally expressed introns and exons by Fisher's exact test. Rows are GO terms, and columns are RF schedules. Enrichment factor was determined as the ratio of diurnal genes in a term over all genes in a term; this is represented by circle size. The color of the circles indicates p value.

(C and D) The expression of the exon and antisense transcripts for two diurnally expressed genes, *Dec2* (C) and *Erc2* (D), featuring diurnally expressed antisense transcripts in all three RF schedules. For *Dec2*, the exon and antisense oscillations are in phase with one another, while for *Erc2*, the exon and antisense have antiphasic oscillations.

initiation of feeding and FT4 and FT8 represent times 4 and 8 hr after the start of feeding.

We identified 2,026 exons differentially regulated by food intake (Figures 4B, S4A, and S4B). Exons showing the most significant change in response to feeding were linked to metabolism (Figure 4C), including *Pdk4*, *Ucp3*, and *Scd2*. The food intake-affected exons fell into two groups: those that decreased (998) after food intake and those that increased (1,028) after food intake (Figures 4B–4E, S4A, and S4B). Genes showing decreased expression after food intake were overrepresented in GO

categories, including response to starvation, autophagy, response to oxidative stress, negative regulation of cell proliferation, and lipid oxidation (Figure 4D; Table S3), and those showing increased expression included lipid biosynthesis and protein synthesis (Figure 4E; Table S3). These results indicate that the metabolism of skin is oxidative before feeding and becomes anabolic after feeding. We also identified 1,890 introns and 662 antisense transcripts affected by food intake (Figures S4A and S4B). About half of the food intake-affected genes were identified as having diurnal expression in one or more of the three feeding
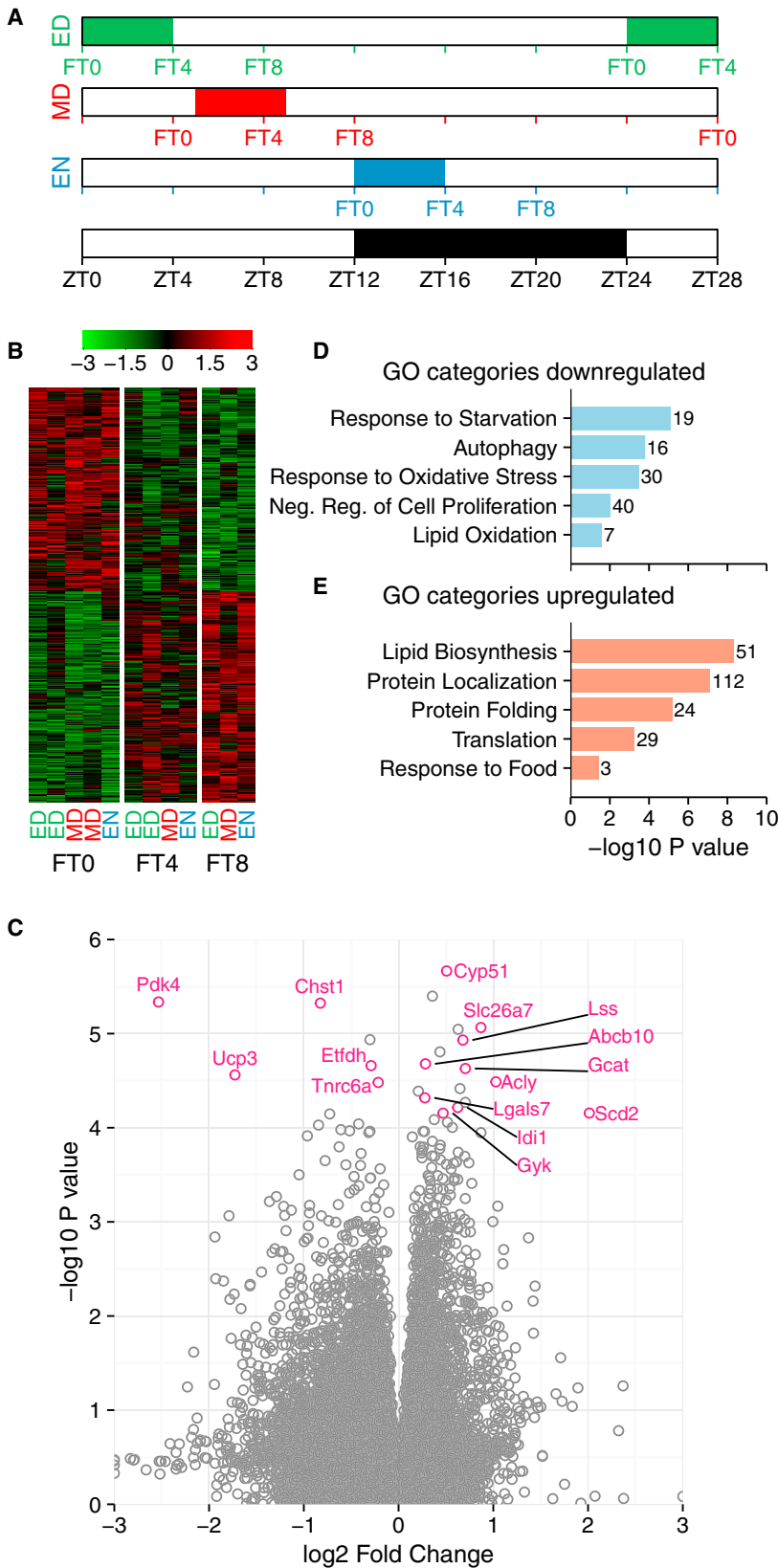
Figure 4. Food Intake Alters the Skin Transcriptome

(A) A schematic showing how the RNA-seq reads from data presented in Figures 2 and 3 were regrouped and analyzed on the basis of the timing of food availability. Feeding time zero (FT0) indicates reads immediately before food availability, feeding time 4 (FT4) indicates reads 4 hr after the onset of food availability, and feeding time 8 (FT8) indicates reads 8 hr after the onset of food availability, as described in Experimental Procedures. Feeding groups are indicated below each column. The white-black bar indicates day and night, respectively.

(B) A total of 2,026 exons were affected by feeding on the basis of the regrouping described in (A) (one-way ANOVA $p < 0.01$). Shown is the heatmap of food intake-affected genes at FT0, FT4, and FT8. The color key represents the Z score of expression value, with red being highly expressed genes and green being minimally expressed genes.

(C) Volcano plot showing feeding-affected exons. Representative, statistically significant metabolic genes are labeled.

(D and E) Graphs of representative enriched GO categories for genes downregulated (D) or upregulated (E) after feeding. The numbers at the end of the bars refer to the number of genes affected in each category.

See also Figure S4 and Table S3.

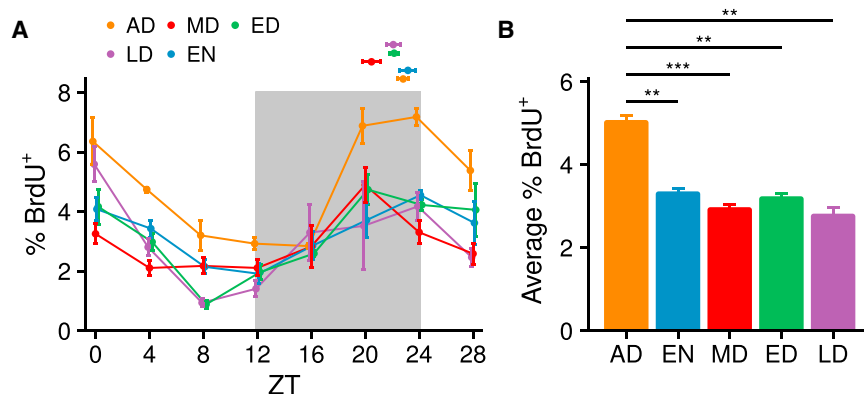schedules (Figure S4C), suggesting that food intake contributes to regulation of the diurnal transcriptome in the skin. In conclusion, these data indicate that expression of many genes in the skin, including those involved in oxidative-reductive metabolism and cell proliferation, respond acutely to food intake, and that the metabolic status of skin is determined by feeding.

RF-Induced Phase Shifts of the Circadian Clock Do Not Affect the Diurnal Phase of Epidermal Progenitor Cell S Phase

Previous studies showed diurnal changes in epidermal progenitor cell proliferation with 3- to 4-fold greater number of cells in S phase during the night than during the day (Geyfman et al., 2012). Deletion of *Bmal1*, either constitutively or selectively in epidermal cells, obliterates the diurnal variation in cell proliferation, indicating that the circadian clock controls the diurnal variation in epidermal progenitor cell proliferation (Geyfman et al., 2012).

To determine whether the RF-induced phase shifts in the skin's circadian clock alter the phase of the diurnal variation in epidermal progenitor cell proliferation, we measured the proportion of epidermal progenitor cells in S phase by BrdU staining over a 28 hr period. The proportion of cells in S phase is diurnal under each of the five RF schedules. Interestingly, despite the different phases in the circadian clock in different RF schedules, the phase of S phase was not shifted by RF (Figure 5A). We also evaluated whether RF affects the proliferation rate of interfollicular epidermal progenitor cells, finding that each of the RF schedules resulted in a similar and decreased peak and overall progenitor cell proliferation compared with AD (Figure 5B). Together with previous findings showing that the circadian clock is required for diurnal DNA synthesis rhythms in epidermal progenitor cells (Geyfman et al., 2012), these results indicate that whereas the clock is critical for establishing diurnal variation in progenitor cell proliferation, it alone does not control the phase of the cell cycle.

Daytime Feeding Shifts Skin Sensitivity to UVB-Induced DNA Damage

Previous work in mice showed that sensitivity to UVB-induced DNA damage in the epidermis is diurnal with more damage

when UVB is applied during the night than during the day (Gaddameedhi et al., 2011; Geyfman et al., 2012). This diurnal variation depends on the circadian clock as mutations in *Bmal1* (Geyfman et al., 2012) and *Cry1/Cry2* (Gaddameedhi et al., 2011) obliterate the diurnal variation. To test whether daytime feeding, with its consequent shift in the phase of the clock, modulates the epidermal sensitivity to UVB-induced DNA damage, we applied UVB during the day (ZT9) and night (ZT21) to the shaved backs of AD, EN, ED, and MD mice, collecting the skin 15 min after UVB exposure. Consistent with previous studies (Gaddameedhi et al., 2011; Geyfman et al., 2012), mice that ate mainly (AD) or only (EN) at night formed more cyclobutane pyrimidine dimers (CPDs) when exposed to UVB during the night than during the day (Figure 6A). In contrast, mice fed during the day (ED and MD) exhibited a reverse pattern, forming more CPDs when exposed to UVB during the day than during the night (Figure 6A). Similar trends were observed in an earlier RF experiment with fewer mice in which we measured both CPDs and the second most common UVB-induced lesion, (6-4) photoproducts ([6-4]PP) (Figure S5). Thus, while not altering the phase of S phase in epidermal progenitor cells, daytime RF reverses the diurnal rhythm of sensitivity to UVB-induced DNA damage. In addition, we found that the expression of *Xpa*, the gene encoding a rate-limiting protein necessary for nucleotide excision repair of UVB-induced DNA (Li et al., 2011; Miyamoto et al., 1992), is dampened in EN, MD, and ED compared with AD. Furthermore, *Xpa* expression oscillates in a diurnal fashion in AD but not as robustly in the RF schedules (Figure 6B).

In sum, these results demonstrate that daytime RF affects the sensitivity to DNA damage in the skin of mice and dampens the expression of a key DNA repair factor.

DISCUSSION

This work shows that time of feeding is an important regulator of skin function. As summarized in Figure 6C, we found that (1) RF shifts the phase of the skin circadian clock, in a pattern distinct from that of the liver; (2) RF alters the expression of many diurnally expressed genes in the skin, including that of the key DNA repair factor *Xpa*; (3) feeding acutely causes large-scale
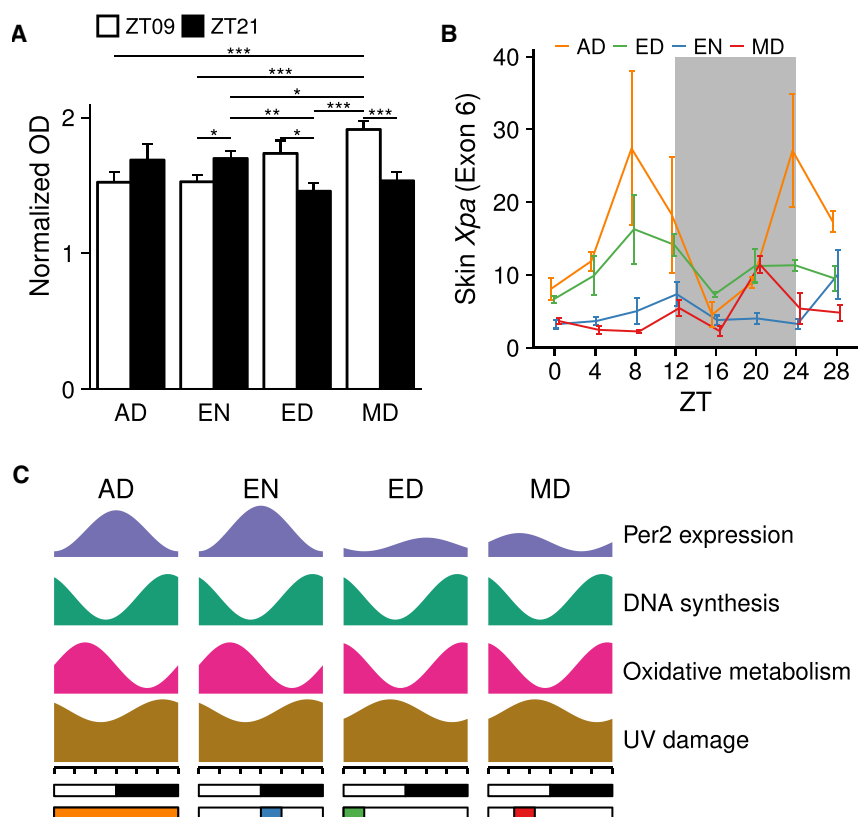
Figure 6. Skin Sensitivity to UVB-Induced DNA Damage

(A) Quantification of CPD photoproducts after UVB exposure at ZT9 and ZT21. The shaved back skins of mice from AD, EN, ED, and MD feeding schedules were exposed to single dose of 500 J/m^2 UVB. Greater UVB-induced DNA damage is seen in AD and EN mice exposed to UVB at night versus the day, while mice fed during the day (ED and MD) have greater UVB-induced DNA damage when exposed to UVB during the day than during the night. Values represent mean ± SEM, n = 15. Statistical significance was determined using Welch's t test, shown as *p < 0.05, **p < 0.01, and ***p < 0.001.

(B) Skin *Xpa* expression is dampened under RF, as detected by qPCR. Values represent mean ± SEM (n = 3–5). Two-way ANOVA shows significance for RF group (p < 0.0001), ZT time (p < 0.002), and RF group X ZT time (p < 0.02). Tukey's post hoc test shows that AD has greater *Xpa* expression compared with EN (p < 0.0001) and MD (p < 0.0001), while AD is not significantly different from ED (p < 0.056).

(C) A schematic summarizing the effects of abnormal feeding time on diurnal rhythms UVB-induced DNA damage, expression of oxidative-reductive metabolic enzymes, DNA synthesis and *Per2* expression.

See also Figures 1, 2, 5, and 6A.

gene expression changes in the skin, most prominently of metabolic genes; and (4) daytime RF reverses the time-of-day-dependent sensitivity to UVB-induced DNA damage in the skin. Together, our results indicate that timing of food intake has a more pronounced influence on skin biology than previously recognized, representing a modifiable regulator of skin health.

Studies focusing on the liver, a key organ for organismal metabolism, showed that the phase of the circadian clock is entrained by RF (Damiola et al., 2000; Kuroda et al., 2012; Stokkan et al., 2001) and that a significant portion of the liver transcriptome is affected by the time of feeding (Vollmers et al., 2009). The effect of RF on clocks in peripheral organs not primarily involved in organismal metabolism is less well studied (Izumo et al., 2014; Reznick et al., 2013); in particular, there are no such studies in the skin. Our findings indicate that both the phase and peak expression of the skin circadian clock are distinct from that of the liver. In the skin, day-fed mice (MD, ED, and LD) exhibit lower amplitude of the core clock gene *Per2* than mice fed during the night (EN), while in the liver, *Per2* amplitude does not seem to be sensitive to time of feeding. Furthermore, mice fed during the ED exhibited a 4.7 hr phase delay in *Per2* expression compared with AD mice in the skin, while in the liver the phase of *Per2* expression is advanced by 10.9 hr, corresponding to the initiation of food intake. These findings suggest that RF controls the phase of the skin circadian clock by different mechanisms than in the liver, where feeding appears to be a more direct and dominant cue (Figure 1). These observations suggest that in addition to regulation of the skin clock by the SCN's central clock

(Tanioka et al., 2009), the skin clock is independently modulated by the timing of food intake. The exact mechanism by which feeding time controls the skin clock likely involves many factors such as physical activity, sleep-wake cycles, metabolism, and circulating hormones.

Comparison of the telogen skin transcriptome under three different RF schedules (ED, MD, and EN) reveals that feeding schedule dictates the diurnal expression of approximately 10% of the skin transcriptome (Figure 2). Specifically, RF schedules generate diurnal gene rhythms that are largely unique to each RF schedule while dampening diurnal expression of other genes that are diurnal in the other RF schedules (Figure 2). Furthermore, while feeding time largely defines the identity of individual genes with oscillating expression, the functional categories annotated to these genes are similar among the three RF schedules. We also found that some diurnally expressed genes are conserved in all the three RF schedules; these genes are enriched for regulators of the circadian clock. The phase shift of the clock-related transcripts under the three RF schedules correlates well with the phase shift of the core circadian clock as indicated by the peak time of *Per2* expression (Figure 1). In addition, the shift of expression of exons is linearly correlated with that of introns, indicating that shift of transcriptional activity is an important mechanism underlying the shift of the whole transcriptome (Figure 3). Genes annotated to regulation of circadian rhythm tend to be diurnally expressed in introns and exons, while some genes annotated to the cell cycle, especially cytokinesis, tend to be diurnally expressed in exons and not introns. These findings suggest that

different diurnal processes may be regulated to varying extents by both transcriptional and/or post-transcriptional mechanisms.

In contrast to exons, there are very few diurnal antisense transcripts. Also, the expression of antisense transcripts is largely uncorrelated with the expression of either introns or exons of the corresponding diurnal genes. We have identified a few antisense genes, however, that exhibit unique diurnal expression in relation to their corresponding genes, indicating a potential regulatory role.

We observed striking changes in skin gene expression directly in response to food intake (Figure 4). This suggests that at least part of the RF schedule-mediated changes in gene expression are a direct feeding effect, although we cannot rule out contributions by changes in rhythms of activity level and sleep caused by restricted food availability. An analysis of these gene expression changes indicates that after feeding, cellular metabolism becomes biosynthetic and reductive. Instead of oxidation of fatty acids, the skin transcriptome becomes more characteristic of the synthesis and import of lipids, especially steroids, which are involved in cellular membrane systems. In addition, in response to food intake, genes involved in transcription, translation, and protein folding and localization are upregulated and those involved in apoptosis are downregulated. This analysis indicates that components of the global diurnal gene expression program are acutely responsive to food intake.

In previous studies, we showed that the circadian clock intrinsic to keratinocytes is required for the diurnal fluctuation in the proportion of epidermal progenitors undergoing S phase (Geyfman et al., 2012). Interestingly, in the present study, we find that despite the shift in the phase of the circadian clock by RF, the rhythm of DNA synthesis in epidermal progenitors of the skin did not shift (Figure 5). Together these findings indicate that while an intact clock is required for the diurnal variation in DNA synthesis, the phase of the clock is not the dominant regulator of the phase of the S phase oscillations in the mouse skin. These findings are in agreement with studies showing that the cell mitotic cycle can be uncoupled from the circadian clock in immortalized rat-1 fibroblasts (Yeom et al., 2010) and Lewis lung carcinoma cells (Pendergast et al., 2010) and a recent study showing that cell division cycles could be gated by WNT-signaling (Matsu-Ura et al., 2016). Although a previous study showed that RF can shift the daily proliferative rhythm of the digestive tract (Burholt et al., 1985), in the gut, cell proliferation may be mechanically stimulated by food.

Given our finding that oxidative metabolism in the skin is affected by RF, it is likely that a deviation in the time of food intake may lead to asynchrony between oxidative metabolism and DNA replication, which normally is coordinated with cell cycle stages in epidermal progenitors (Stringari et al., 2015). We hypothesize that such asynchrony between the timing of peak oxidative phosphorylation metabolism and cell division due to unusual feeding times could contribute to increased ROS-mediated DNA damage in progenitor and stem cells, leading to aging and carcinogenesis.

We also show that feeding at non-physiological times can alter the skin's susceptibility to UVB-induced DNA damage. Mice that eat during the normal time (night) have greater sensitivity to UVB-induced DNA damage at night compared with during the day,

consistent with previous studies (Figure S5; Geyfman et al., 2012; Gaddameedhi et al., 2011). This rhythm in DNA damage is attributed to the increased number of progenitors undergoing S phase at night (Geyfman et al., 2012) and the diurnal variation in the efficacy of DNA excision repair mediated by the key nucleotide excision repair factor Xpa (Gaddameedhi et al., 2011). We found that daytime-fed mice had reversed diurnal rhythm of sensitivity to UVB-induced DNA damage with greater sensitivity during the day than during the night (Figure 6A). Because phase of S phase is not altered by RF, other factors may contribute to the RF-altered rhythm in the susceptibility to DNA damage. In fact, the expression of the key repair gene Xpa is diurnal, peaking during the day in AD mice (Figure 6B) (Gaddameedhi et al., 2011; Kang et al., 2010) but exhibiting dampened and less rhythmic expression under RF schedules (Figure 6B).

In conclusion, our findings show that RF (EN, ED, and MD) decreases the proportion of cells in S phase and dampens expression of DNA repair factor Xpa. In addition to these changes, daytime RF (ED and MD) also shifts the phase of core clock genes and oxidative metabolism genes and reverses the rhythm of sensitivity to UVB-induced DNA damage. By disrupting the natural expression and diurnal variation of such important processes in the skin, abnormally timed food intake may contribute to the development of skin pathologies involving sun damage, skin aging, and skin cancer.

EXPERIMENTAL PROCEDURES

Animals

Twenty-three-day-old male C57BL/6NCrl mice (strain code 027; Charles River Laboratories) were acclimated to the mouse facility for 1–2 weeks before starting the RF experiments. The mice were housed under 12 h/12 h light/dark cycles (light on at 6:30 am, ZT0, and off at 6:30 pm, ZT12) with free access to water during the whole experiment and free access to food before initiation of the RF experiments. Regular chow was used in all experiments. The RF schedules were carried out for 18–21 days for the RNA-seq, qPCR, and cell proliferation experiments (the first RF experiment) and 21–26 days for the DNA damage and body weight/food intake data (the second RF experiment). In the first RF experiment, EN mice had free access to food from ZT12 for 4 hr during the first 8 days but after that were given the same amount food as was eaten by ED mice. Slight modifications to the RF schedules in the second RF experiment were as follows. The mice were weighed every other day immediately prior to daily food availability. Each day, ED and MD mice were given access to 20 g of chow for 4 hr, and leftover food was measured. The average food consumed per mouse in ED and MD was given to EN mice beginning at ZT12. Because EN mice ate all the food they received during the first 4 hr of food availability, EN food intake (Figure S1A) was represented as the food weight they received. In both experiments, skin was sampled at the end of the experiment during the second telogen, when mice were at around postnatal day 54; the telogen state of the skin was verified by histology. All procedures were approved by the Institutional Animal Care and Use Committee of the University of California, Irvine (approval number 2001-2239).

Cell Proliferation Assays

Four hours prior to sampling, 50 μg/g BrdU was injected intraperitoneally. The histological staining for BrdU was performed as previously described (Geyfman et al., 2012). BrdU-positive and BrdU-negative cells were quantified using ImageJ with the observer blind to experimental conditions.

Quantitative PCR

Total RNA from whole dorsal back skin was purified with TRIzol Reagent (Life Technologies), cDNA was synthesized with iScript cDNA Synthesis Kit (Bio-Rad), and qPCR was performed with SsoFast EvaGreen/Probes Supermix

(Bio-Rad). The Taqman probes for *Per2* (Mm00478113.m1) and the *Xpa* probe detecting exons 2–3 (Mm00457111_m1) were from Applied Biosystems. Primers for *Per1* and *Dbp* were from PrimerBank (Wang et al., 2012b) (ID: 26349399a1 for *Per1* and 8393240a1 for *Dbp*). The *Xpa* primer sequences for the last exon (exon 6) of *Xpa* are (5′–3′) ATTGCGGCGAGCAATAAGAAG and ACAAGGTACAAGTCTTGCGGT, from Eurofins.

Statistics on qPCR and Cell Proliferation
The biological replicates of each time point of each RF schedule were assigned to four sets of artificial time series by random permutation, and the peak time, mean, and peak expression of each time series was calculated with the cosinor function of psych package (Revelle, 2016). The peak value was calculated as mean × (1 + amplitude). The phase shift between any two RF schedules was calculated using the peak time of the curves in the same set, so that four replicates of the peak time, average value, peak value, and peak shift were produced at each permutation. The calculation of the mean and SD of peak time as well as the Watson-Williams test of difference between peak time means and between the shifts was done with the circular package (Agostinelli and Lund, 2013). The calculation and test were done for 100 permutations, and the average of the mean, SEM, and the p values were presented.

Stranded Total RNA Sequencing
Total RNA from mouse whole back skin with RNA integrity number (RIN) higher than 6.5 were pooled, treated with RNase-Free DNase (catalog no. 79254; QIAGEN), and cleaned with RNeasy Mini Elute Cleanup Kit (QIAGEN). The library was constructed with TruSeq Stranded Total RNA Sample Prep Kit (Illumina) and sequenced with Hiseq 2500 (Illumina).

Analysis of RNA-Seq Data
RNA-seq short reads were mapped to mouse genome mm10 by Tophat2 (Kim et al., 2013), and rRNA reads were removed from the bam file via RSeQC (Wang et al., 2012a). The reads with mapping quality less than 5 were removed using SAMtools (Li et al., 2009) (Table S1). Then the exon and intron gene reads and the reads for the antisense region of the whole gene body were counted using HOMER (Heinz et al., 2010). Transcripts were annotated using the UCSC known canonical gene set (31,872 total, 22,526 with introns). The reads were normalized into RPKM (reads per kilobase per million) using CQN (Hansen et al., 2012). The data analysis thereafter was performed using R (Ihaka and Gentleman, 1996; R Core Team, 2014), if not differently specified.

Identification of Diurnal Genes
Circadian genes identified in each of four algorithms, ARSER (Yang and Su, 2010), Lomb-Scargle (Glynn et al., 2006; Lomb, 1976), JTK-Cycle (Hughes et al., 2010), and sinusoid curve fitting (Geyfman et al., 2012), were combined to generate one circadian gene list. The exon reads from EN were ranked by the p value of each method and compared with the genes circadian in telogen skin (Geyfman et al., 2012), or circadian in at least seven other tissues (Yan et al., 2008). The ratio of reference genes (positive found ratio [PFR]) was found within a sliding window of 100 genes moving from the top (most significant p values) for each method. Then, the PFRs of each method's list were smoothed using the loess function in R base. A p value cutoff was chosen for each method so that the smoothed PFR was high enough to be significant compared with a random ordering of genes, using a permutation test with a p value cutoff of p < 0.01. These cutoffs were applied to all transcripts for each method, and transcripts identified by at least one of these methods were incorporated into the final circadian list. Because each algorithm has pros and cons (Deckard et al., 2013), combining the different methods using PFR to determine the cutoffs in a consistent way yielded a more comprehensive circadian list. The peak time predicted by Lomb-Scargle method (Glynn et al., 2006; Lomb, 1976) was adopted for the phase shift analysis.

Identification of Feeding-Affected Genes
Whole-skin RNA-seq exon reads from EN, ED, and MD were re-grouped according to the feeding time (FT0 being the onset of feeding, FT4 being 4 hr after the onset of feeding, FT8 being 8 hr after the onset of feeding, for each partic-ular RF schedule) and then averaged. Feeding-affected genes were identified by comparing RNA-seq expression values at FT0 (ZT4 and ZT28 for MD, ZT12 for EN, ZT0 and ZT24 for ED), FT4 (ZT8 for MD, ZT16 for EN, ZT4 and ZT28 for ED), and FT8 (ZT12 for MD, ZT20 for EN, ZT8 for ED) using one-way ANOVA. The higher ratio among the FT8/FT0 and FT4/FT0 ratios was used to represent the fold change in gene expression after feeding.

Functional Enrichment Analysis
GO annotations were downloaded on October 1, 2014, from EBI (ftp://ftp.ebi.ac.uk/pub/databases/GO/goa/MOUSE/gene_association.goa_mouse.gz) and MGI (ftp://ftp.informatics.jax.org/pub/reports/gene_association.mgi). Annotations were combined to get a more comprehensive list of gene sets. Fisher's exact test was used for enrichment test, and the IEA annotations were included.

UVB-Induced DNA Damage Assays
Two days before the end of the RF experiment, mice were anesthetized by intraperitoneal injection of ketamine (100 mg/kg) and xylazine (10 mg/kg), and then their back skin was shaved using electric clippers during a time that would not interfere with their feeding schedules. A single dose of 500 J/m^2 was applied to the mice 15 min before sampling as described previously (Geyfman et al., 2012), at ZT9 or ZT19. Whole back skin DNA was isolated with QIAamp DNA Mini Kit (catalog no. 51306; QIAGEN). ELISA was used to detect CPDs and (6-4)PP and with antibodies from Cosmo Bio (NMDND001 for CPDs and NMDND002 for [6-4]PPs) following the manufacturer's protocol.

Skin Histology Measurement
The dorsal skin of the mice used in the second RF experiment was collected, fixed in 10% formalin for 48 hr, ethanol-dehydrated, and embedded in paraffin. After sectioning, dewaxing, and rehydrating, staining with hematoxylin and eosin was performed. Twenty-fold magnified mosaic images were acquired on a Keyence microscope, with at least 1,000 μm skin length per image. Histological measurements were performed by a blinded researcher using ImageJ software. At least two images per mouse were analyzed, and 15 measurements for each skin compartment per image were averaged.

ACCESSION NUMBERS
The accession number for the RNA-seq data reported in this paper is GEO: GSE83855.

SUPPLEMENTAL INFORMATION
Supplemental Information includes five figures and three tables and can be found with this article online at http://dx.doi.org/10.1016/j.celrep.2017.07.022.

AUTHOR CONTRIBUTIONS
H.W., E.V.S., M.G., V.K., N.L., J.S.T., and B.A. conceived and designed the experiments. H.W., E.V.S., and M.G. performed the experiments. H.W., E.V.S., Q.L., M.L.S., A.I., and B.A. analyzed the data. H.W. made the figures with suggestions from all the authors. H.W., E.V.S., and B.A. wrote the manuscript with input from all of the authors.

REFERENCES

Adamovich, Y., Rousso-Noori, L., Zwighaft, Z., Neufeld-Cohen, A., Golik, M., Kraut-Cohen, J., Wang, M., Han, X., and Asher, G. (2014). Circadian clocks and feeding time regulate the oscillations and levels of hepatic triglycerides. Cell Metab. 19, 319–330.

Agostinelli, C., and Lund, U. (2013). R package 'circular': circular statistics (version 0.4-7). https://r-forge.r-project.org/projects/circular/.

Armstrong, B.K., and Kricker, A. (2001). The epidemiology of UV induced skin cancer. J. Photochem. Photobiol. B 63, 8–18.

Bass, J. (2012). Circadian topology of metabolism. Nature 491, 348–356.

Blanpain, C., and Fuchs, E. (2009). Epidermal homeostasis: a balancing act of stem cells in the skin. Nat. Rev. Mol. Cell Biol. 10, 207–217.

Buchakjian, M.R., and Kornbluth, S. (2010). The engine driving the ship: metabolic steering of cell proliferation and death. Nat. Rev. Mol. Cell Biol. 11, 715–727.

Burholt, D.R., Etzel, S.L., Schenken, L.L., and Kovacs, C.J. (1985). Digestive tract cell proliferation and food consumption patterns of Ha/ICR mice. Cell Tissue Kinet. 18, 369–386.

Damiola, F., Le Minh, N., Preitner, N., Kornmann, B., Fleury-Olela, F., and Schibler, U. (2000). Restricted feeding uncouples circadian oscillators in peripheral tissues from the central pacemaker in the suprachiasmatic nucleus. Genes Dev. 14, 2950–2961.

Deckard, A., Anafi, R.C., Hogenesch, J.B., Haase, S.B., and Harer, J. (2013). Design and analysis of large-scale biological rhythm studies: A comparison of algorithms for detecting periodic signals in biological data. Bioinformatics 29, 3174–3180.

Dibner, C., Schibler, U., and Albrecht, U. (2010). The mammalian circadian timing system: organization and coordination of central and peripheral clocks. Annu. Rev. Physiol. 72, 517–549.

Fisher, G.J., Kang, S., Varani, J., Bata-Csorgo, Z., Wan, Y., Datta, S., and Voorhees, J.J. (2002). Mechanisms of photoaging and chronological skin aging. Arch. Dermatol. 138, 1462–1470.

Fritz, V., and Fajas, L. (2010). Metabolism and proliferation share common regulatory pathways in cancer cells. Oncogene 29, 4369–4377.

Gaddameedhi, S., Selby, C.P., Kaufmann, W.K., Smart, R.C., and Sancar, A. (2011). Control of skin cancer by the circadian rhythm. Proc. Natl. Acad. Sci. U S A 108, 18790–18795.

Geyfman, M., Kumar, V., Liu, Q., Ruiz, R., Gordon, W., Espitia, F., Cam, E., Millar, S.E., Smyth, P., Ihler, A., et al. (2012). Brain and muscle Arnt-like protein-1 (BMAL1) controls circadian cell proliferation and susceptibility to UVB-induced DNA damage in the epidermis. Proc. Natl. Acad. Sci. U S A 109, 11758–11763.

Gillette, M.U., and Sejnowski, T.J. (2005). Physiology. Biological clocks coordinately keep life on time. Science 309, 1196–1198.

Glynn, E.F., Chen, J., and Mushegian, A.R. (2006). Detecting periodic patterns in unevenly spaced gene expression time series using Lomb-Scargle periodograms. Bioinformatics 22, 310–316.

Hansen, K.D., Irizarry, R.A., and Wu, Z. (2012). Removing technical variability in RNA-seq data using conditional quantile normalization. Biostatistics 13, 204–216.

Hara, R., Wan, K., Wakamatsu, H., Aida, R., Moriya, T., Akiyama, M., and Shibata, S. (2001). Restricted feeding entrains liver clock without participation of the suprachiasmatic nucleus. Genes Cells 6, 269–278.

Heinz, S., Benner, C., Spann, N., Bertolino, E., Lin, Y.C., Laslo, P., Cheng, J.X., Murre, C., Singh, H., and Glass, C.K. (2010). Simple combinations of lineage-determining transcription factors prime cis-regulatory elements required for macrophage and B cell identities. Mol. Cell 38, 576–589.

Hughes, M.E., Hogenesch, J.B., and Kornacker, K. (2010). JTK_CYCLE: an efficient nonparametric algorithm for detecting rhythmic components in genome-scale data sets. J. Biol. Rhythms 25, 372–380.

Ihaka, R., and Gentleman, R. (1996). R: a language for data analysis and graphics. J. Comput. Graph. Stat. 5, 299–314.

Izumo, M., Pejchal, M., Schook, A.C., Lange, R.P., Walisser, J.A., Sato, T.R., Wang, X., Bradfield, C.A., and Takahashi, J.S. (2014). Differential effects of light and feeding on circadian organization of peripheral clocks in a forebrain Bmal1 mutant. eLife 3, 3.

Janich, P., Pascual, G., Merlos-Suárez, A., Batlle, E., Ripperger, J., Albrecht, U., Cheng, H.Y., Obrietan, K., Di Croce, L., and Benitah, S.A. (2011). The circadian molecular clock creates epidermal stem cell heterogeneity. Nature 480, 209–214.

Jouffe, C., Cretenet, G., Symul, L., Martin, E., Atger, F., Naef, F., and Gachon, F. (2013). The circadian clock coordinates ribosome biogenesis. PLoS Biol. 11, e1001455.

Kang, T.H., Lindsey-Boltz, L.A., Reardon, J.T., and Sancar, A. (2010). Circadian control of XPA and excision repair of cisplatin-DNA damage by cryptochrome and HERC2 ubiquitin ligase. Proc. Natl. Acad. Sci. U S A 107, 4890–4895.

Kim, D., Pertea, G., Trapnell, C., Pimentel, H., Kelley, R., and Salzberg, S.L. (2013). TopHat2: accurate alignment of transcriptomes in the presence of insertions, deletions and gene fusions. Genome Biol. 14, R36.

Kondratov, R.V., Kondratova, A.A., Gorbacheva, V.Y., Vykhovanets, O.V., and Antoch, M.P. (2006). Early aging and age-related pathologies in mice deficient in BMAL1, the core componentof the circadian clock. Genes Dev. 20, 1868–1873.

Kuroda, H., Tahara, Y., Saito, K., Ohnishi, N., Kubo, Y., Seo, Y., Otsuka, M., Fuse, Y., Ohura, Y., Hirao, A., and Shibata, S. (2012). Meal frequency patterns determine the phase of mouse peripheral circadian clocks. Sci. Rep. 2, 711.

Lamia, K.A., Papp, S.J., Yu, R.T., Barish, G.D., Uhlenhaut, N.H., Jonker, J.W., Downes, M., and Evans, R.M. (2011). Cryptochromes mediate rhythmic repression of the glucocorticoid receptor. Nature 480, 552–556.

Laporte, D., Lebaudy, A., Sahin, A., Pinson, B., Ceschin, J., Daignan-Fornier, B., and Sagot, I. (2011). Metabolic status rather than cell cycle signals control quiescence entry and exit. J. Cell Biol. 192, 949–957.

Levi, F., and Schibler, U. (2007). Circadian rhythms: mechanisms and therapeutic implications. Annu. Rev. Pharmacol. Toxicol. 47, 593–628.

Lévi, F., Filipski, E., Iurisci, I., Li, X.M., and Innominato, P. (2007). Cross-talks between circadian timing system and cell division cycle determine cancer biology and therapeutics. Cold Spring Harb. Symp. Quant. Biol. 72, 465–475.

Li, H., Handsaker, B., Wysoker, A., Fennell, T., Ruan, J., Homer, N., Marth, G., Abecasis, G., and Durbin, R.; 1000 Genome Project Data Processing Subgroup (2009). The Sequence Alignment/Map format and SAMtools. Bioinformatics 25, 2078–2079.

Li, Z., Musich, P.R., Serrano, M.A., Dong, Z., and Zou, Y. (2011). XPA-mediated regulation of global nucleotide excision repair by ATR Is p53-dependent and occurs primarily in S-phase. PLoS ONE 6, e28326.

Lin, K.K., Kumar, V., Geyfman, M., Chudova, D., Ihler, A.T., Smyth, P., Paus, R., Takahashi, J.S., and Andersen, B. (2009). Circadian clock genes contribute to the regulation of hair follicle cycling. PLoS Genet. 5, e1000573.

Lomb, N.R. (1976). Least-squares frequency analysis of unequally spaced data. Astrophys. Space Sci. 39, 447–462.

Lowrey, P.L., and Takahashi, J.S. (2011). Genetics of circadian rhythms in mammalian model organisms. Adv. Genet. 74, 175–230.

Masri, S., Cervantes, M., and Sassone-Corsi, P. (2013). The circadian clock and cell cycle: interconnected biological circuits. Curr. Opin. Cell Biol. 25, 730–734.

Matsu-Ura, T., Dovzhenok, A., Aihara, E., Rood, J., Le, H., Ren, Y., Rosselot, A.E., Zhang, T., Lee, C., Obrietan, K., et al. (2016). Intercellular coupling of the cell cycle and circadian clock in adult stem cell culture. Mol. Cell 64, 900–912.

Miyamoto, I., Miura, N., Niwa, H., Miyazaki, J., and Tanaka, K. (1992). Mutational analysis of the structure and function of the xeroderma pigmentosum group A complementing protein. Identification of essential domains for nuclear localization and DNA excision repair. J. Biol. Chem. 267, 12182–12187.

Mohawk, J.A., Green, C.B., and Takahashi, J.S. (2012). Central and peripheral circadian clocks in mammals. Annu. Rev. Neurosci. *35*, 445–462.

Panda, S., Antoch, M.P., Miller, B.H., Su, A.I., Schook, A.B., Straume, M., Schultz, P.G., Kay, S.A., Takahashi, J.S., and Hogenesch, J.B. (2002). Coordinated transcription of key pathways in the mouse by the circadian clock. Cell *109*, 307–320.

Pendergast, J.S., Yeom, M., Reyes, B.A., Ohmiya, Y., and Yamazaki, S. (2010). Disconnected circadian and cell cycles in a tumor-driven cell line. Commun. Integr. Biol. *3*, 536–539.

Plikus, M.V., Vollmers, C., de la Cruz, D., Chaix, A., Ramos, R., Panda, S., and Chuong, C.M. (2013). Local circadian clock gates cell cycle progression of transient amplifying cells during regenerative hair cycling. Proc. Natl. Acad. Sci. U S A *110*, E2106–E2115.

Plikus, M.V., Van Spyk, E.N., Pham, K., Geyfman, M., Kumar, V., Takahashi, J.S., and Andersen, B. (2015). The circadian clock in skin: implications for adult stem cells, tissue regeneration, cancer, aging, and immunity. J. Biol. Rhythms *30*, 163–182.

R Core Team (2014). R: a language and environment for statistical computing. R Foundation for Statistical Computing, https://www.r-project.org/.

Revelle, W. (2016). psych: Procedures for Psychological, Psychometric, and Personality Research. https://CRAN.R-project.org/package=psych.

Reznick, J., Preston, E., Wilks, D.L., Beale, S.M., Turner, N., and Cooney, G.J. (2013). Altered feeding differentially regulates circadian rhythms and energy metabolism in liver and muscle of rats. Biochim. Biophys. Acta *1832*, 228–238.

Stokkan, K.A., Yamazaki, S., Tei, H., Sakaki, Y., and Menaker, M. (2001). Entrainment of the circadian clock in the liver by feeding. Science *291*, 490–493.

Stringari, C., Wang, H., Geyfman, M., Crosignani, V., Kumar, V., Takahashi, J.S., Andersen, B., and Gratton, E. (2015). In vivo single-cell detection of metabolic oscillations in stem cells. Cell Rep. *10*, 1–7.

Tanioka, M., Yamada, H., Doi, M., Bando, H., Yamaguchi, Y., Nishigori, C., and Okamura, H. (2009). Molecular clocks in mouse skin. J. Invest. Dermatol. *129*, 1225–1231.

Vollmers, C., Gill, S., DiTacchio, L., Pulivarthy, S.R., Le, H.D., and Panda, S. (2009). Time of feeding and the intrinsic circadian clock drive rhythms in hepatic gene expression. Proc. Natl. Acad. Sci. U S A *106*, 21453–21458.

Wang, L., Wang, S., and Li, W. (2012a). RSeQC: quality control of RNA-seq experiments. Bioinformatics *28*, 2184–2185.

Wang, X., Spandidos, A., Wang, H., and Seed, B. (2012b). PrimerBank: a PCR primer database for quantitative gene expression analysis, 2012 update. Nucleic Acids Res. *40*, D1144–D1149.

Yan, J., Wang, H., Liu, Y., and Shao, C. (2008). Analysis of gene regulatory networks in the mammalian circadian rhythm. PLoS Comput. Biol. *4*, e1000193.

Yang, R., and Su, Z. (2010). Analyzing circadian expression data by harmonic regression based on autoregressive spectral estimation. Bioinformatics *26*, i168–i174.

Yeom, M., Pendergast, J.S., Ohmiya, Y., and Yamazaki, S. (2010). Circadian-independent cell mitosis in immortalized fibroblasts. Proc. Natl. Acad. Sci. U S A *107*, 9665–9670.

Yoon, J.A., Han, D.H., Noh, J.Y., Kim, M.H., Son, G.H., Kim, K., Kim, C.J., Pak, Y.K., and Cho, S. (2012). Meal time shift disturbs circadian rhythmicity along with metabolic and behavioral alterations in mice. PLoS ONE *7*, e44053.

Supplemental Information

Time-Restricted Feeding Shifts

the Skin Circadian Clock

and Alters UVB-Induced DNA Damage

Hong Wang, Elyse van Spyk, Qiang Liu, Mikhail Geyfman, Michael L. Salmans, Vivek Kumar, Alexander Ihler, Ning Li, Joseph S. Takahashi, and Bogi Andersen
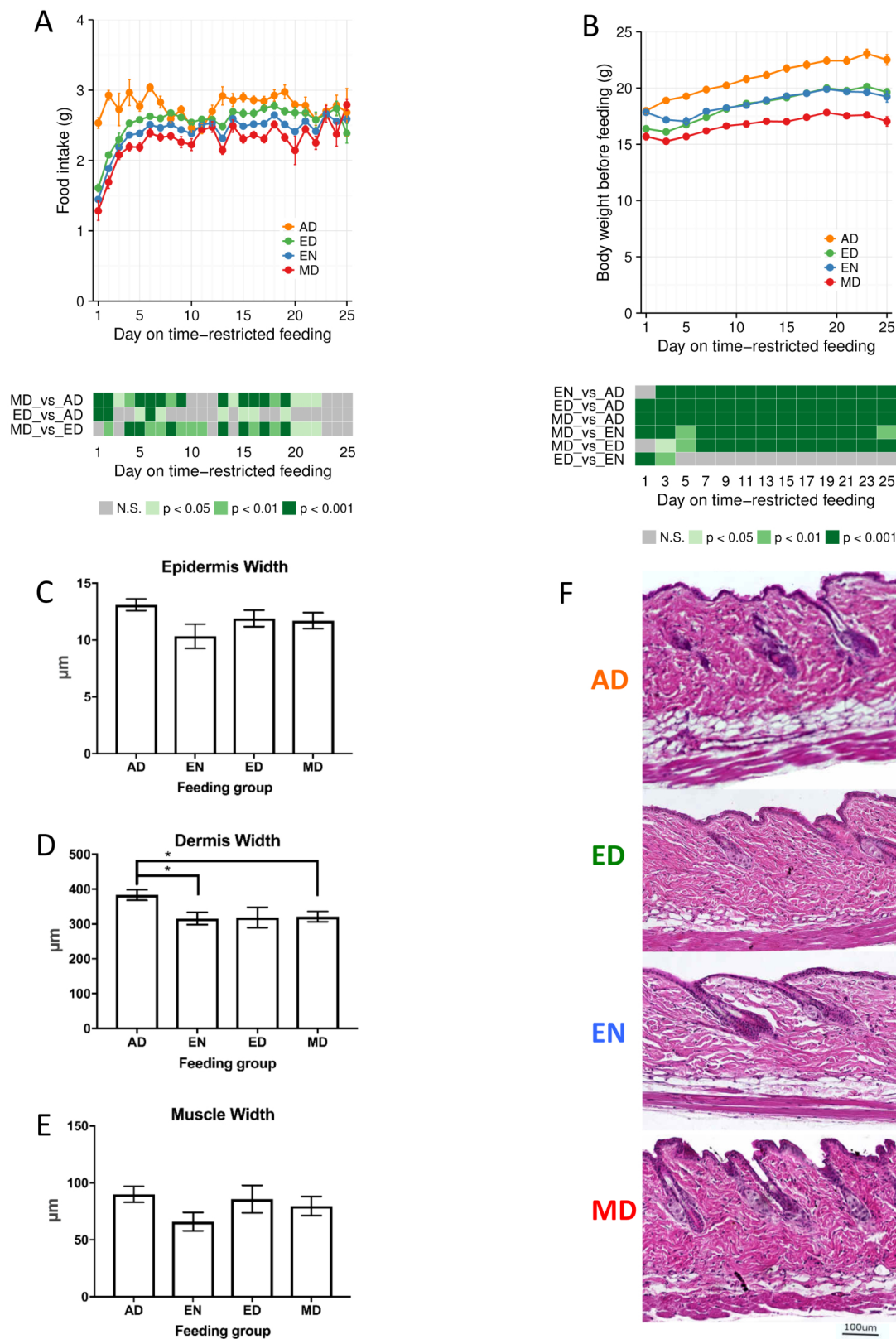
Figure S1. Food intake, body weight, and skin histology after RF schedules, Related to Figure 1

(A) Food intake throughout the RF protocol. Two-way ANOVA (Group × Time): RF schedule (p < 0.001), ZT time (p < 0.001) and RF schedule × ZT time (p < 0.001). Data are represented as mean ± SEM, N = 15-18. (B) Body weights throughout the RF protocol. Two-way ANOVA: RF schedule (p < 0.001), ZT Time (p < 0.001) and RF schedule × ZT time (p < 0.001). Data are represented as mean ± SEM, N = 11-36. For (A) and (B), Welch's t-test p-values comparing feeding groups at each timepoint are listed below the graphs. Shade of green indicates significance, with darker green being more significant. (C-E) Skin histology measurements. Skin was collected, paraffin embedded, sectioned and stained with hematoxylin and 20x mosaic images were acquired. The thickness of (C) epidermis, (D) dermis (including the intradermal fat layer), and (E) subcutaneous muscle were measured. Data is presented as Mean ± SEM for N=10-18 mice per group. Significance was determined by one-way ANOVA (only dermis showed significance with P= 0.03), followed by Student's paired t-test, shown as *p < 0.05. (F) Representative cropped images of skin histology from the RF groups quantified in C-E. 100 um scale bar is shown.
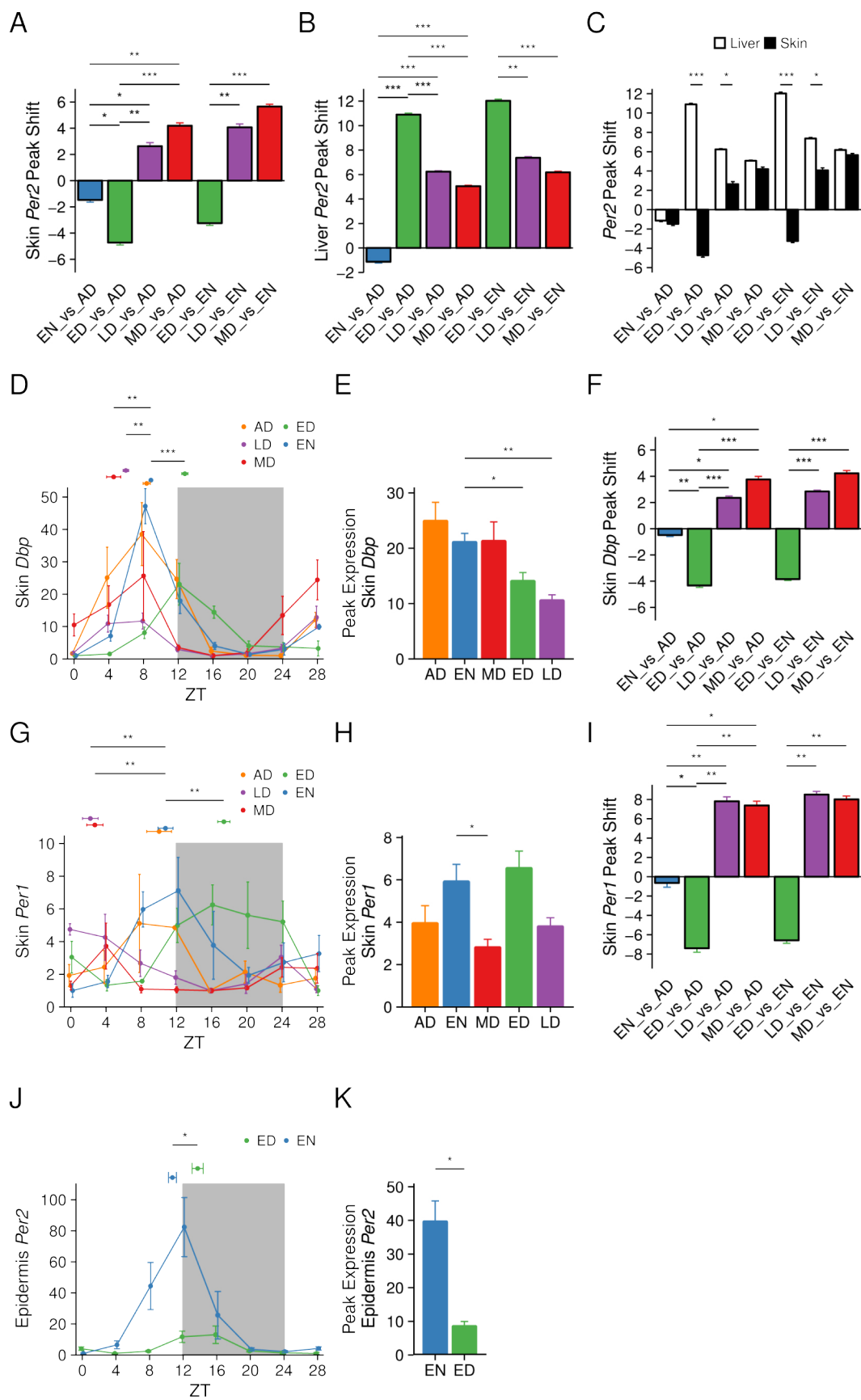
Figure S2. *Per2*, *Dbp* and *Per1* expression and comparison of peak shifts, Related to Figure 1

(*A*) Peak shift of skin *Per2* expression. (B) Peak shift of liver *Per2* expression. (C) Comparison of peak shifts of *Per2* expression in skin and liver. (D) *Dbp* gene expression in the skin measured by qPCR. (E) Peak expression of skin *Dbp*. (F) Comparison of the peak shifts of skin *Dbp* expression. (G) *Per1* gene expression in the skin measured by qPCR. (H) Peak expression of skin *Per1*. (I) Comparison of peak shifts of skin *Per1* expression. (J) *Per2* gene expression in the epidermis measured by qPCR. (K) Peak expression of epidermis *Per2*. (D, G, J) QPCR data is represented as mean ± SEM N = 3-5, after removal of outliers (Dixon's Q test, $Q_{99\%}$). The peak time of each group is shown above the curves represented as mean ± SEM N = 4. Watson-Williams test was used to compare the peak times (A-D, F, G, I, J) and Welch's t-test was used to peak expression levels (E, H, K). (A-K) For peak time and peak expression, the values represent mean ± SEM, N = 4. Statistical significance shown as *p < 0.05, **p < 0.01, *** p < 0.001.
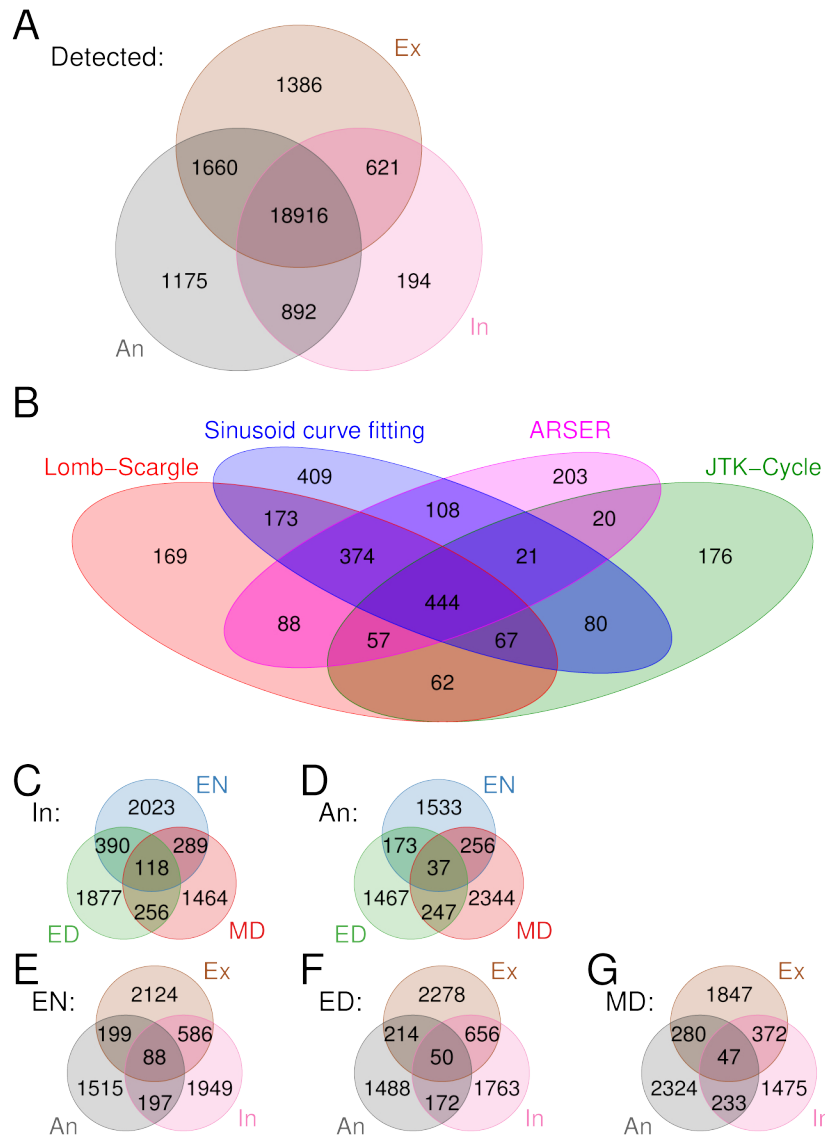
Figure S3. Identification of diurnal transcripts, Related to Figure 2

(A) Overlap of detected exons, introns and antisense transcripts. (B) Overlap of diurnal exons of EN identified by different algorithms. Genes identified as diurnal by any algorithm(s) are included. (C-D) Overlap of diurnal introns (C) and antisense (D) transcripts in three feeding groups. (E-G) Overlap of diurnal transcripts in EN (E), ED (F) and MD (G) (A and C-G) Ex: exons; An: antisense; In: introns.
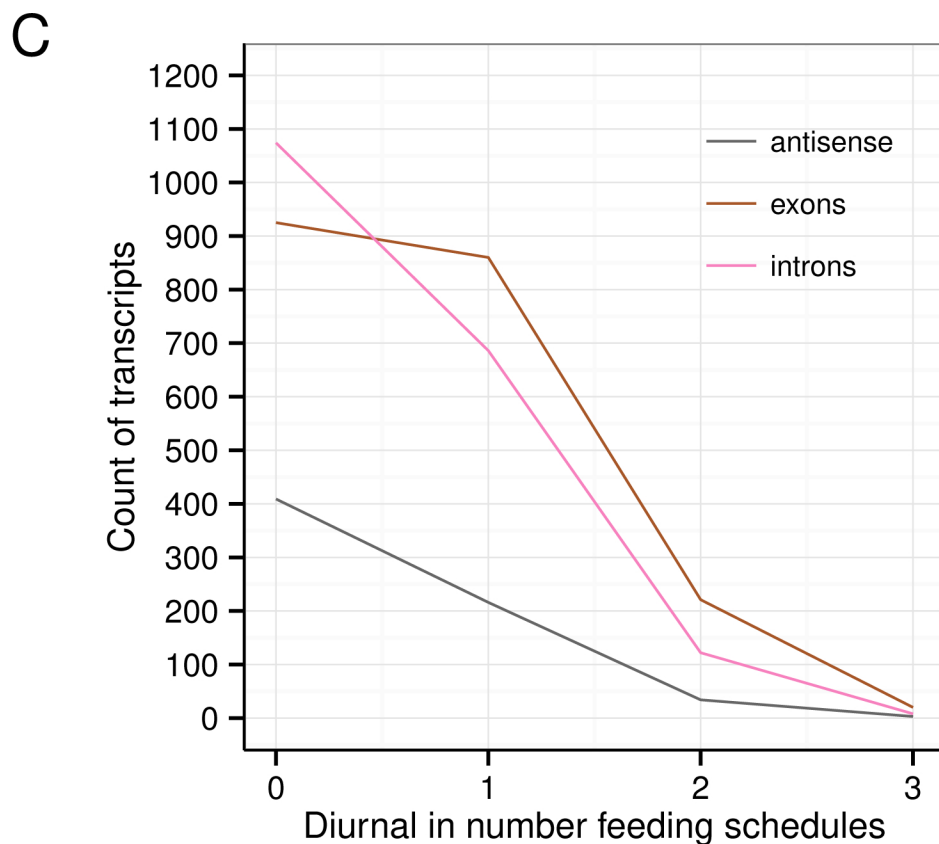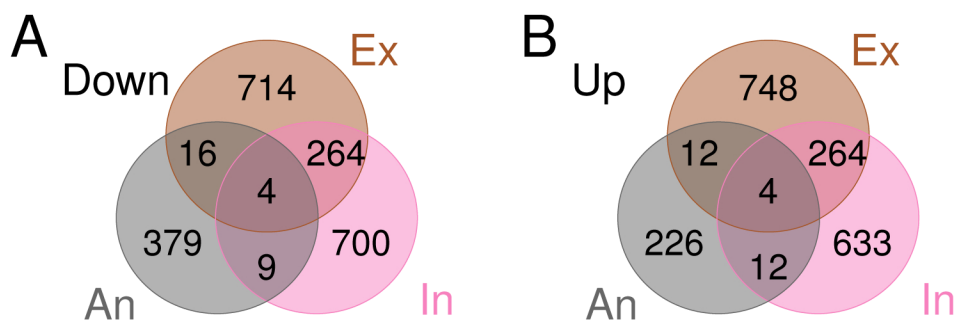
Figure S4. Genes affected by food intake, Related to Figure 4

(A) Overlap of transcripts downregulated after feeding. (B) Overlap of transcripts upregulated after feeding. (A-B) Ex: exons; An: antisense; In: introns. (C) Graph depicting the number of feeding-affected transcripts that were identified as diurnal in 0, 1, 2, or 3 of the feeding groups.
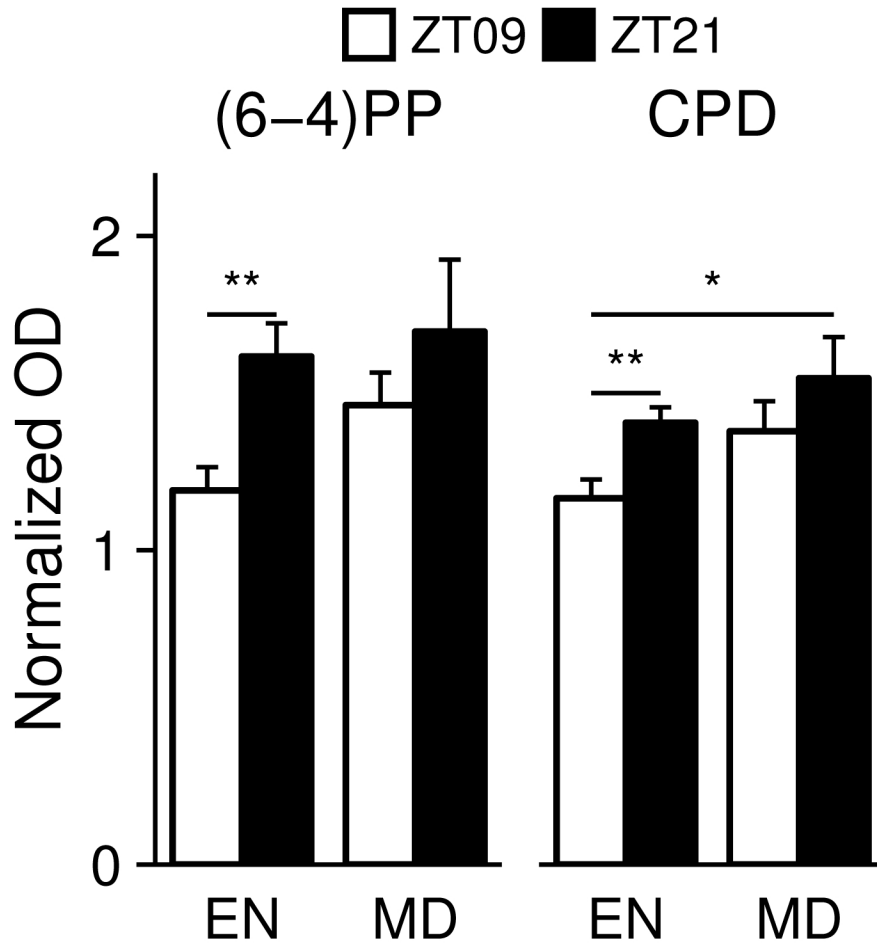
Figure S5. Skin sensitivity to UVB-induced DNA damage, Related to Figure 6
Quantification of (6-4)PP (left) and CPD (right) photoproducts after UVB exposure at ZT9 and ZT21 presented as Mean ± SEM (N = 8 or 9). Statistical significance was determined by Welch's t-test, shown as *p < 0.05, **p < 0.01, *** p < 0.001.

Table S1. Sequencing statistics for the RNA-seq, Related to Figure 2

Total reads, Mapped reads, percentage of reads mapped, non-rRNA reads, percentage of non-rRNA reads, reliable reads, and percentage of reliable reads, are indicated for RNA samples pooled from 2-4 mice per feeding group per time point as described in Methods section.

RNA sample		Total Reads	Mapped Reads	%	Non-rRNA Reads	%	Reliable Reads	%
MD	ZT0	53934987	50643956	94	47875030	89	43454124	81
	ZT4	58618045	51192377	87	46375200	79	39297337	67
	ZT8	63095384	52605332	83	44237151	70	33523750	53
	ZT12	56033285	48428388	86	41704141	74	31765142	57
	ZT16	59424906	52510958	88	46931580	79	38730040	65
	ZT20	63122441	53106139	84	47206698	75	37788061	60
	ZT24	58323439	51335336	88	47077225	81	41369525	71
	ZT28	53651833	47565580	89	42935111	80	36460548	68
ED	ZT0	64957607	56059860	86	50466217	78	39190824	60
	ZT4	62418183	52613181	84	45941760	74	33349770	53
	ZT8	63370673	53849389	85	46528867	73	32703877	52
	ZT12	54188794	45372675	84	38868470	72	24701796	46
	ZT16	59349340	47636646	80	41538428	70	27724999	47
	ZT20	61264210	53695629	88	48245655	79	35409323	58
	ZT24	53567052	45183962	84	39463990	74	25666218	48
	ZT28	64239934	52534714	82	45068850	70	32519483	51
EN	ZT0	63221149	50308240	80	43408139	69	28029993	44
	ZT4	60383655	51373718	85	43435890	72	30094176	50
	ZT8	62202466	53013034	85	46199673	74	31599842	51
	ZT12	67298866	54763533	81	46887244	70	29689138	44
	ZT16	59099629	47049092	80	39259630	66	25012802	42
	ZT20	99558258	80519391	81	69863732	70	47313932	48
	ZT24	59662234	47684780	80	40522893	68	27120354	45
	ZT28	63367104	50211616	79	41047157	65	26751407	42